https://doi.org/10.5194/egusphere-2024-3840
Preprint. Discussion started: 14 January 2025

Sea Ice Screening Ability in Ku Band and C Band Wind Scatterometry

Xingou Xu[1], Ad Stoffelen[2]

[1]The CAS Key Laboratory of Microwave Remote Sensing, National Space Science Center, Chinese Academy of Sciences, Beijign, 100190, China
[2] Satellite Observations, Royal Netherlands Meteorology Institute, De Bilt, 3730 AE, the Netherlands

Correspondence to: Ad Stoffelen (ad.stoffelen@knmi.nl)

Abstract. Ocean surface sea ice screening is important for a wide variety of research and applications. While the normalized radar cross-sections (NRCS) have been long applied in sea ice classifications and quantifications, the beam-filling problem still exists. Besides, for the melting ice cover, the NRCS are not providing accurate links to sea ice. However, if considering the NRCS within the traditional wind retrieval unit, despite the existence of fractal sea ice and the different mixing quantities of ice and sea water, there will be signatures in both the derivations from wind retrieval model and the extend of heterogeneity within the unit. The former has been well researched and together with the ice model from scatteroemters, applied now in ice labelling for scatterometer operational wind products in the indicator *MLE*. In this research, we uncover the properties of the later due to sea ice, in terms of the indicator J_{oss}. The sea ice and iceberg concentration from products derived in AMSR-2 and Sentinel-1 are applied as references. The scatterometer data are from collocations of C- and Ku-band scatterometer products from ASCAT-A, ASCAT-B, OSCAT-2 and HSCAT. The ice screening ability in combination of MLE and J_{oss} are concluded. Finally, the iceberg identification potential is discussed along with the application of the joint observations of C- and Ku-band scatteroemter observations.

1 Introduction

Sea ice plays a relevant role in connection with short-term climate variations between the large amount of parameters in the cryosphere by affecting the Earth's radiation budget in terms of altering the albedo of the ocean surface (Pistone K. et al., 2014). It can also interact with the actions between the air and water result in a different sea surface feature when exist and move with the wind or ocean surface currents (Timmermans M.-L. and Marshall J., 2020; Haumann A., 2011). The descriptions of the sea ice are then vital for both understanding the cryosphere and measurement involving it (Sandven, S., et al., 2023; Wernecke, A. et al., 2024). In open seas and along the coastal regions in high latitudes, it can be generally quantified by sea ice concentration (SIC) (Melsheimer, C., 2018), when including floating large icebergs, the iceberg concentration is applied (Buus-Hinkler, J., 2023). As the existence of sea ice, either in a wide coverage or scatter over the ocean, surveillance over a wide range is effective and can be realized by remote sensing techniques (Sandven, S., et al.,

https://doi.org/10.5194/egusphere-2024-3840
Preprint. Discussion started: 14 January 2025

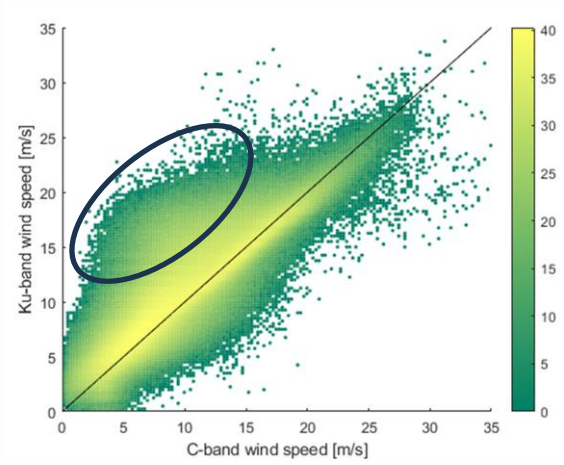

(a)

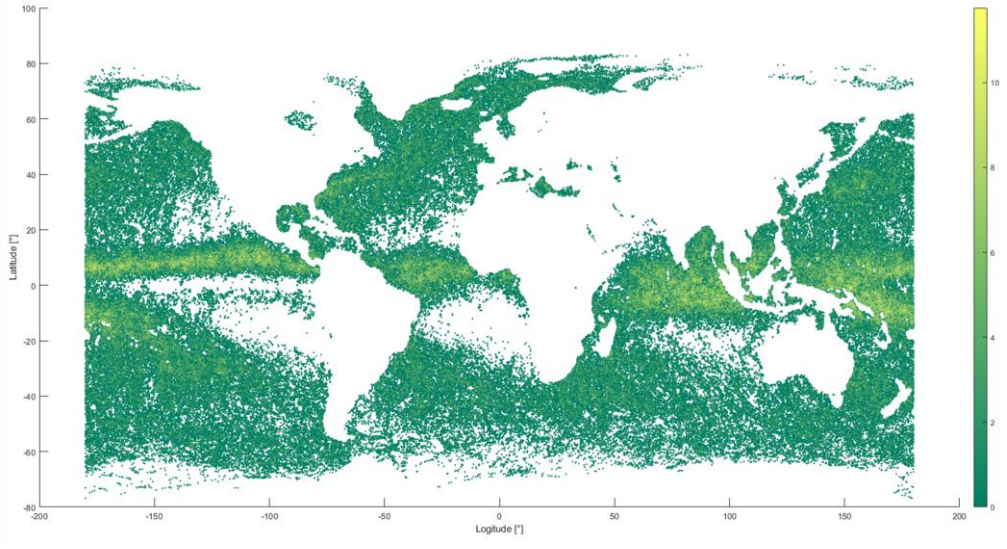

(b)

Figure 1 The collocated C-band acceptance and Ku-band QC rejected WVCs in MLE metrics: (a) is the wind panel (b) is the density map from J_{oss} metrics in (Xu X. and Stoffelen A., 2020), roughly in correspondence to the circled WVC in (a). The blank region in (b) are without data corresponding to good quality from MLE QC and those of land regions (M_Map, 2003). Color indicate density in dB.

2006). Among all them, Active microwave remote sensing has been well applied owe to their good stability and accuracy in the measurements. Though designed and applied for ocean surface measurements, Scatterometer has been well applied for ocean surface remote sensing for more than 40 years, it also has been well applied for ice remote sensing for about more than 30 years (Vogelzang, J., and Stoffelen, A., 2012; Ricciardulli L. and Wentz F. J. 2015). They generally work at C or Ku band. The measured normalized backscattering coefficients from scatterometers can provide information of ice types of different

https://doi.org/10.5194/egusphere-2024-3840
Preprint. Discussion started: 14 January 2025

ice age, as the NRCS has good relation with different ice in varied ages that are with different structures (Drinkwater, M. R., et al., 1995; Belmonte Rivas, M., 2018, Woodhouse I., 2006). However, when the NRCS are mapped to SIC, especially for low SIC cases, the uncertainties in quantification become large (Haarpaintner, J., et al., 2004). This is generally due to errors from the mixed characteristics of backscattering mechanism involving melting mixed ice and water, as well as the same reason induced errors in the SIC products that are usually applied as estimation references.

Meanwhile, as scatterometers observe wind in the square-grid spatial unit known as wind vector cells (WVC), that are formed in a way with several NRCS obtained in different azimuth geometry assembled for wind direction estimation (magazine paper). With multiple observations, optimal wind field can be estimated in the maximum likelihood estimation (Portabella, M., 2002; Portabella, M., and Stoffelen, A., 2002). During such procedure, the model applied mapping winds to different observations are the Geophysical Model Functions (GMF) (Wentz, F. J., et al., 1984; Stoffelen A. et al., 2017). Meanwhile, the estimator defined in the MLE procedures as the Euclidean distance from wind GMF, i.e. the MLE estimators (MLE) label the deviation from pure wind model that are induced by the unmodelled factors such as convective rains, existence of sea ice (Stoffelen A., 1998). When refer specifically to sea ice, ice GMFs have also been developed for mapping pure ice features to scatterometer observed NRCS (Belmonte Rivas, M., 2018; Lindell, D. B. and Long, D. G; 2016a; Lindell, D. B. and Long, D. G; 2016b). Although NRCS from pure ice are not changing with azimuth geometry, and the mapping is still from NRCS to ice features of ice age categories, together with wind GMFs in MLE, they can be applied to open sea and coastal regions, by employing the Bayesian procedure for wind values and sea ice existence providing at the same time the optimal estimation probability of both results to improve the wind estimation accuracy (Belmonte R. M. et al., 2012; Otosaka, I., et al., 2018). MLE to wind GMF at the same time, provide also information of the deviation of wind scene to sea ice, and applied as the metrics for quality flag in the quality control (QC) for wind products (Portabella, M. et al., 2010; Verhoef, A. et al., 2012). But the quantitative relation between MLE and SIC and IBC have not been investigated yet.

Furthermore, there is another QC indicator J_{oss}, that compensates MLE by describing the heterogeneity within a WVC. It was proposed inertially for rain screening for tropical regions in wind scatterometry (Xu X. and Stoffelen A., 2020), while now has been well applied for QC in operational global wind products (Xu X., et al., 2021; Stoffelen, A. and Verhoef A., 2021). Since C band is of wavelength about 5.3 centimetre (cm), Ku band is about 2.2cm, C band is less affected by the heterogeneity within the scene. As an example, Figure 1 plots the collocated C-band acceptance and Ku-band QC rejected WVCs in MLE metrics from ASCAT onboard Metop series and OSCAT-2 onboard SCATSAT-1 obtained in about two years. In panel (a), the red circled part is roughly obtained by J_{oss} criteria in (Xu X. and Stoffelen A., 2020) and the density is displayed globally in (b) accumulating this long time-span. For higher latitudes, the heterogeneity can be caused by existence of sea ice when the precipitation is less frequent than tropical regions (Siedler, G. et al., 2001), while specific research on the possible J_{oss} contribution to sea ice distribution features are not yet existed.

In this research, the definition of MLE and J_{oss} as well as how they can be functioning as QC indicators for both C and Ku band scatterometers are reviewed, then with SIC and IBC products, their abilities of in ice screening are extensively investigated, with the differences in SIC and IBC addressed and a special case of iceberg provided. To decimating between

https://doi.org/10.5194/egusphere-2024-3840
Preprint. Discussion started: 14 January 2025

the rain effect, collocated rain information is also obtained for analysing. Results indicate that MLE and J_{oss} illustrate different features against SIC and IBC, due to different representative scale of the two indicators. Their screening and preliminary quantification abilities against ice are identified, concluding an optimal way of combining both indicators in addition to the existing direct mapping to ice from observed NRCS. This research for the first time addresses the effective information for sea ice from sources other than the directly observed NRCS alone, and provide a potential way to obtained better SIC or IBC estimation for future research and applications. The combination analysing of J_{oss} and MLE in Ku and C band also provide hints for further QC method for the dual frequencies scatteroemters.

2 Method

The scatterometer observed NRCS from different azimuth geometry are ensembled within a WVC for wind estimation. For obtaining sea ice information, this also provides opportunities for improving the current sea ice information obtained directly linking the NRCS to pure ice, when the QC indicators can be applied. Generally, MLE and J_{oss} are tow well applied QC indicator in wind scatterometery that are compensating each other (Xu X. et al., 2021; Stoffelen A. and Verhoef A., 2021), The former is already appeared in the optimization procedures of existing estimations employing Bayesian estimation.

2.1 The QC Indicators

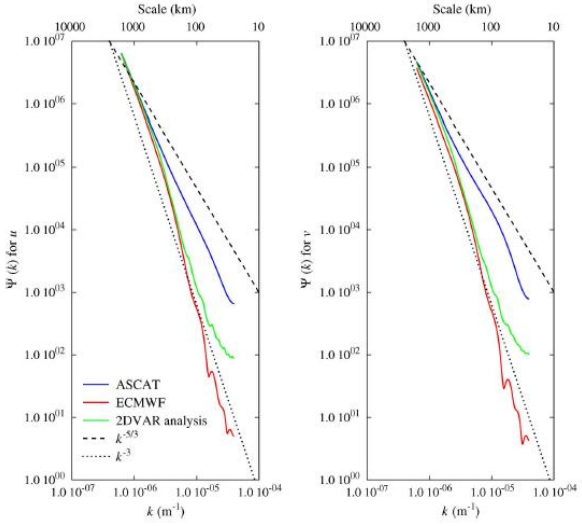

Figure 2: Wind component (u and v) spectra obtained from all ASCAT-12.5 data of January 2009 (Vogelzang, J et al., 2011). The ASCAT (blue solid lines) are at the upper position closet to the 3-D turbulence scale, ECMWF red lines are the solid lines closest to the 2-D scale, while the 2DVAR analysis spectrum (green solid lines) is in between.

The existence of geophysical factors other than wind for a roughened sea surface in the observation scene would deviate the NRCS from the wind GMF and trigger QC rejections. During which, the QC indicators' values are applied as references.

https://doi.org/10.5194/egusphere-2024-3840
Preprint. Discussion started: 14 January 2025

The most utilized is the *MLE*, which is the sum of the normalized Euclidean distances of the observations to the wind GMF sphere, and is expressed in the following equation (Portabella, M., and Stoffelen, A., 2002):

$$MLE = \frac{1}{N}\sum_i^N \frac{(\sigma_i^o - \sigma_i^{sim})^2}{(K_{pi}\cdot\sigma_i^o)^2} \quad (1)$$

In (1), *N* indicate the number of observed NRCS in a WVC, and *MLE* is the average of differences from observations to simulations weighted by the variance of the *i*th NRCS. The simulations are obtained with the estimated wind from the GMF. While pure ice is not changing with azimuth, the distances represented by MLE of the observed NRCS to wind GMF can be deviated by the ice features in the scene. In addition, from the definition, though MLE is weighted average, it is representing the NRCS features within the WVC, without blurring by the adjacent units.

Complimentary to *MLE*, J_{oss} was proposed to describe the heterogeneity of the WVC as the locally perceived wind speed in a WVC differs from the wind speed obtained from neighbouring WVC in the 2-Dimensional Variational Ambiguity Removal (2DVAR) analysis for the Ku-band wind scatterometers (Vogelzang, J et al., 2011; Vogelzang, J. 2019; Xu X. and Stoffelen A., 2020). Figure 2 from (Vogelzang, J et al., 2011) illustrates the wind component spectra obtained from all ASCAT-12.5 data of January 2009. It generally demonstrated that a variational data assimilation scheme based on statistical interpolation acts as a low-pass filter. According to Kolmogorov theory, $k^{(-5/3)}$ is the 3-Dimensional (3-D) energy distribution line, and the larger slope of power(-1/3) is the 2-Dimensional (2-D) energy distribution (Frisch, U., 1995). In Figure 2, the bluelines (upper solid lines) is closer to the 3D smaller scale and descends by the end at the scale for non-linear energy dispassion while the green lines (middle solid lines) do not. Then the indicator J_{oss} defined in the following equation locates and quantifies local disturbances (Xu X. and Stoffelen A., 2020):

$$J_{OSS} = f_o - f_s \quad (2)$$

In (2), f_s is the 2DVAR analysis wind speed at a WVC, f_o is the local WVC-selected wind speed. From (2) and Figure 2, J_{oss} represents the scale difference, then by applying the analysis speed obtained using the NWP information, the spatial representative scale is smaller than MLE when the calculations involving only the observational speed. On the other hand, with the spatial averaging effect, J_{oss} is less noisy than MLE. Furthermore, as J_{oss} is obtained from 2DVAR procedure, this indicator is not available yet for the fixed fan beam C band ASCAT.

Except for rains, the existence of sea ice can also introduce heterogeneity within the WVC. Thus the investigation as well as joint applications of *MLE* and J_{oss} can be further interpretated for high latitudes.

2.2 Method to investigate the sea ice information in the QC indicators

In order to investigate the sea ice information in the QC indicators in open-sea and coastal regions, the reference products of SIC and IBC are applied. For discrimination of rain effects, the collocated rain products are also acquired. During the analysis, after the data collocation, by analysing the distribution plots of the sea ice parameters and MLE by sorting the QC indicator J_{oss}, the ice screening and iceberg identification abilities can be obtained. During this procedure, for further

https://doi.org/10.5194/egusphere-2024-3840
Preprint. Discussion started: 14 January 2025

decimating between information from the rain and ice, the collocated C and Ku band observations are adopted. As the C band corresponds to a wavelength of 5.3 cm while Ku band as about 2.2 cm, C band suffers seldomly rain effects. Then the investigation collocations in C band acceptance and Ku band rejection, as well as both irrespective from flag of the other, can help concluding the ice effect in higher latitudes. Moreover, when the ice screening abilities have been confirmed, the criteria for rain screening are tested if they can fit into the ice features and applied globally. This will in turn contribute to the existing sactterometer QC system.

3 Data and Collocation

The C-band scatterometer data are from the ASCAT-A and ASCAT-B onboard the METOP series, the Ku-band observations collocated with the C-band are obtained from OSCAT-2 onboard the SCATSAT, and the SIC is from the Advanced Microwave Scanning Radiometer-2 (AMSR2) products (Melsheimer C., 2018; 'AMSR2', website accessed 2024), meanwhile, rain rates are from GPM high quality reprocessed final-run products (Huffman G. J., 2015), the iceberg information is acquired from the products from the synthetic aperture radar (SAR) onboard the Sentinel-1 satellite (Buus-Hinkler J., et al., 2023; Sentinel-1, online accessed: 2024-11-11). The scatterometer data and products are obtained by the KNMI processor, with SST effects corrected for the Ku-band (Verhoef A. et al., 2017; Wang Z. et al., 2017). Then the collocated data ranges from October 2016 to January 2019. The collocations are obtained by registering all data to the Ku-band WVC centers. For scatterometers, the time differences of C band are less than 30 minutes, distance lag is less than 25 km. The time differences to the rain reates are within 4.8 minutes. The rain rate values are determined by the area collocating a WVC by averaged in weights (Xu X. et al., 2020). Notably, the SIC is a slowly changed variable that can change within a few days, then their daily information applied, with distance lag set as 12.5km, and the polar projection complicates the retrieval of the intersection areas. The registered SIC values are obtained in the same area-weighting method as for rain rates. The IBC is collocated directly by averaging the samples located within a WVC as the resolution of IBC product from SAR observations are of the scales of kilometres, and are smaller than the WVC size of 25km. In addition, scatterometers detect more sea ice in the melting season than the passive microwave observations from AMSR2, as the latter cannot well distinguish water from water-infested sea ice surfaces. However, the long-term statistics are applied instead of distinguishing the varied seasonal spans for the convenience of future applications.

In all, there are 11,502,621 collocations are obtained with SIC with the C- and Ku-band collocations, where 559,111 WVCs have simultaneous rain rates, among which, 28,068 WVCs are MLE-based KNMI processing flag rejections in the Ku band refection but C band collocation acceptance QC category, and 527,770 WVCs are both accepted by the C- and Ku-band products in MLE-QC.

For the Ku band scatterometers, as seldomly WVC can be collocated with IBC from the collocated C- and Ku-band data set, the statistical features of IBC are obtained in the collocations with the Ku band scatterometer HSCAT onboard the HY-2B

https://doi.org/10.5194/egusphere-2024-3840
Preprint. Discussion started: 14 January 2025

satellite (HY-2B Satellite, online accessed 2024-11-11), covering the year 2019. There are 58 426 WVCs obtained of HSCAT with SIC, IBC and rains collocations for the MLE rejection category.

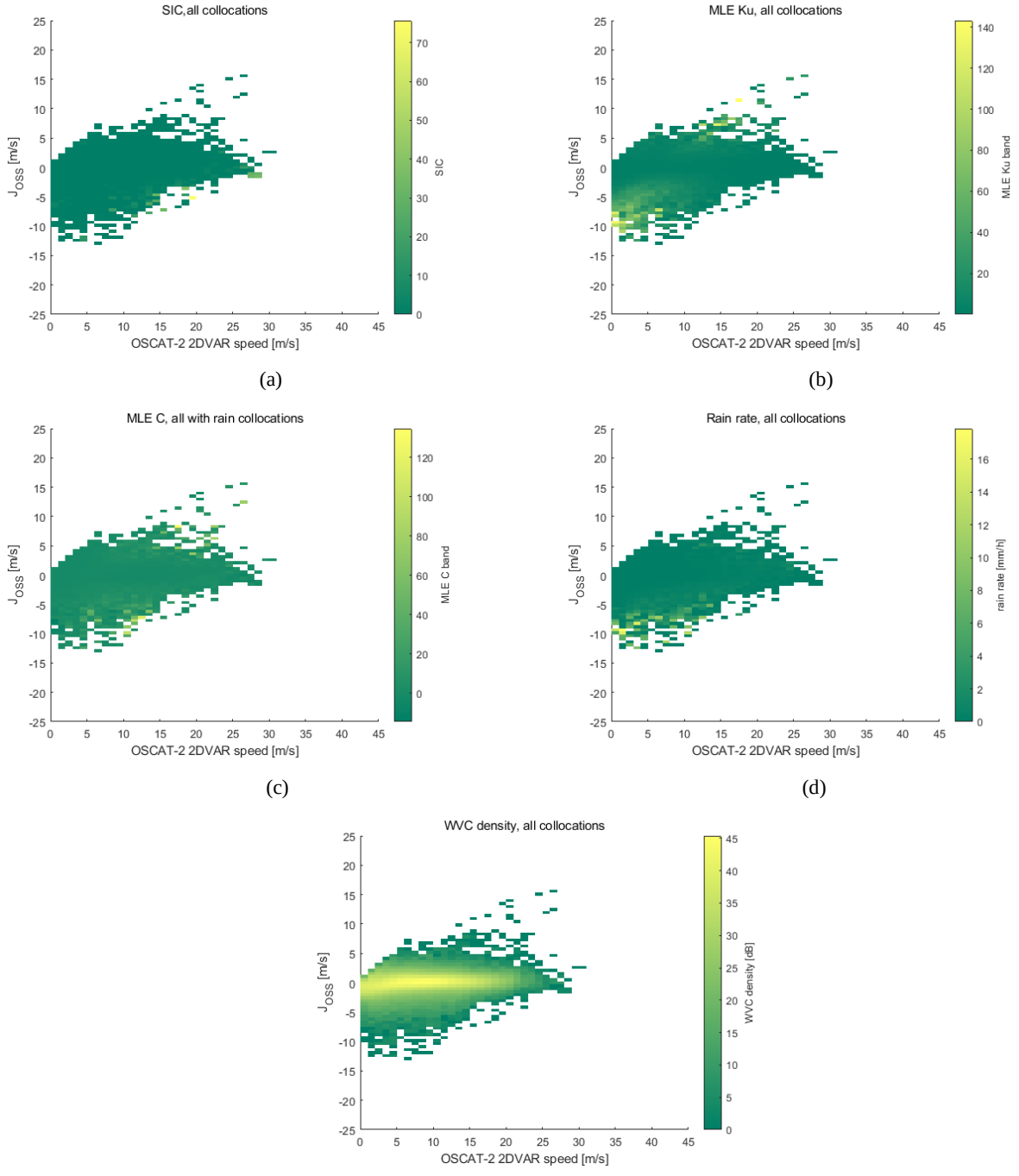

Figure 3 The SIC, MLE values in Ku band, in C band and Ku band J_{oss} values in color in (a), (b), (c) and (d) respectively for the C and Ku band collocations. (e) demonstrates the density of WVC samples in dB.

https://doi.org/10.5194/egusphere-2024-3840
Preprint. Discussion started: 14 January 2025

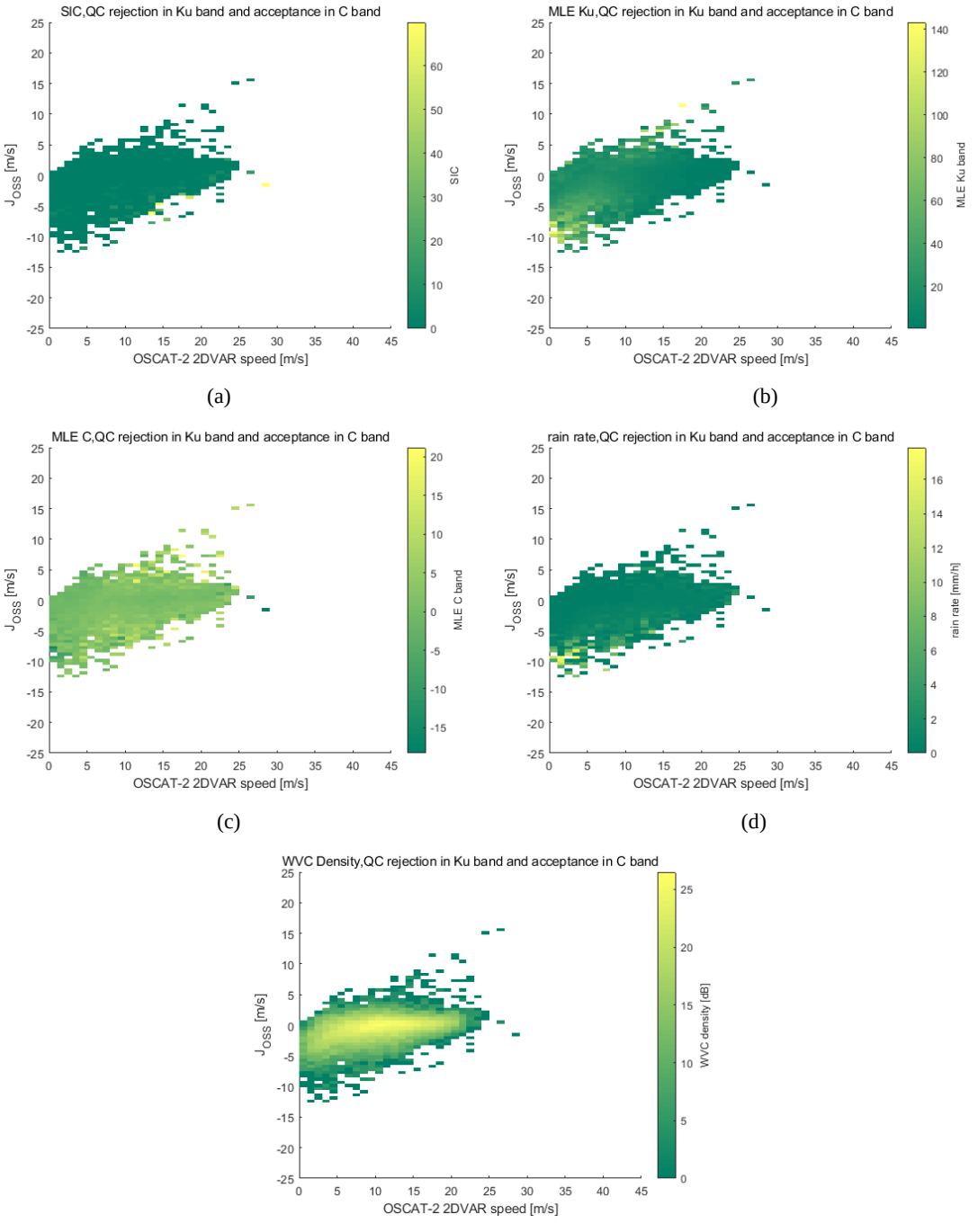

Figure 4 The same setting as in Figure 3 in (a) – (e), but for the MLE QC rejections in Ku band while acceptance in C

https://doi.org/10.5194/egusphere-2024-3840
Preprint. Discussion started: 14 January 2025

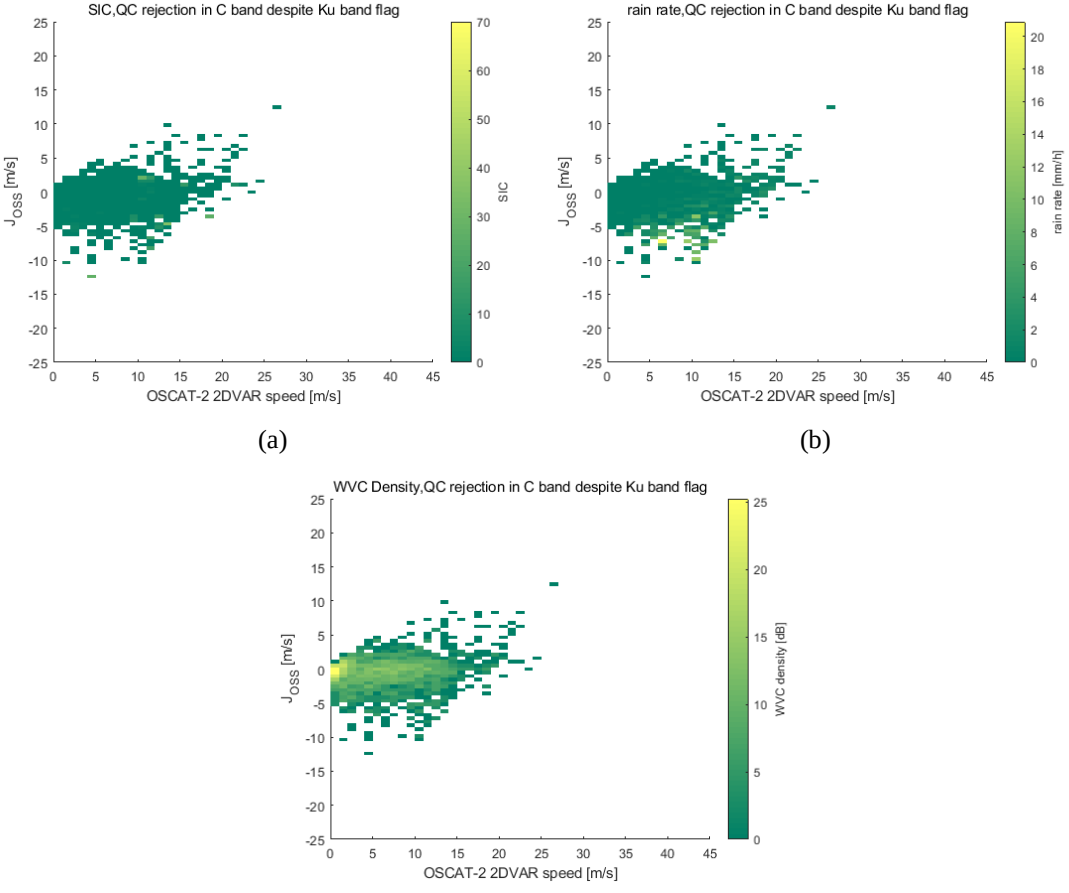

Figure 5 The SIC, rain rate and WVC density in MLE QC rejections of C band.

4 Ice screening ability

The ice screening ability from QC indicators are investigated in terms of SIC and IBC collocations. Both collocations are with simultaneous rain information while the former with also C band collocations. To further discrimination with rains, the collocations with C band acceptance and Ku band rejections, are compared.

4.1 SIC collocation results

Figure 3 illustrate from panel (a) to (d) the SIC, MLE values in Ku band, in C band and J_{oss} values from Ku band in color respectively. The horizontal axis is the 2DVAR speed from the Ku band OSCAT-2, that comprised between observations

https://doi.org/10.5194/egusphere-2024-3840
Preprint. Discussion started: 14 January 2025

and NWP, less affected by heterogeneity within the WVC, thus applied as the *true* wind. The data is sorted by the Joss values in the vertical axis. To confirm the validity of statistics, the WVC density is also displayed in panel (e). the indicator Joss shows good ice screening ability sorting SIC values as well as its different characteristics with MLE. The density displayed in (e) illustrates that the statistics are quite independent with sample amount. Notably, the sea ice feature in SIC is well sorted by J_{oss} and gather well along with 2DVAR wind speed. Rains are generally well screened in J_{oss} (Stoffelen A. and Verhoef A., 2021), however, when compare (a) and (d) in both figures, the differences in distribution of SIC and rain can be observed in the Ku rejection with similar properties in Figure 2. This is consistency to the differences in rain and ice induced NRCS alternation than wind: the former are generally crowded to a certain value for different polarizations while for varied SIC, NRSC varies (Haarpaintner, J., 2004). From (a) and (d), significant SIC samples are appearing at higher 2DVAR speed than rains. Specifically, it can be observed from (a) and (d), SIC affect observations less often than for rains, while for the 2DVAR speed larger than 11 m/s, SIC effects cannot be observed for positive J_{oss}, which forms a different feature with rains for J_{oss}. In addition, with the different patterns of (b) and (c) to (a), the complementary feature of J_{oss} to MLE flags is also evident. From (a) to (d), MLE performs good in identifying rains and SIC, both C and Ku band MLE are more sensitive to SIC than rains, while C-band MLE is more likely to be linked with sea ice than rains for its longer wavelength that can penetrate rains while the larger sea ice coverage can still vary the signals. To further discriminate between rain, the Ku band MLE QC rejection and C band acceptance in the collocation is filtered and display in Figure 4.

When comparing Figure 3 and Figure 4, the density distributions in panel (e) demonstrate the rejections, with different color axis maximums indicating the effective in rejection. As the rain patterns in (d) for both figures vary little, then the C band QC is not affected much by rains, from the validity of existing C band QC in MLE metrics, the immune of C band scatteroemters to rain contaminations are also confirmed. Meanwhile, in (a) and (d), it is also indicated the false alarms exist in the QC- rejection, consistency to the existing QC applications of employing J_{oss} and MLE, confirms the validation of the method to sea ice case. Furthermore, the SIC and rain panels in (a) and (d) in both figures, where the most of the bright samples are included indicating further that Ku band are not only affected severer by rain but also by SIC than C band. This is further demonstrated in Figure 5, where the C band rejections are illustrated despite the Ku band flag for SIC and rain panels and corresponding density in (a), (b) and (c) respectively. For better display, the color scales are different from those in Figure 3 and Figure 4. From (a) and (b) in Figure 5, C band rejections are not well related to rains or SIC, this can also be identified from the maximums shown in the color bars, when the density in (c) shows that the features are not related with sample numbers.

4.2 IBC collocation results

Figure 6 demonstrate the IBC, SIC, rain rates, MLE in the Ku-band HSCAT onboard HY-2B satellite. The sample densities respectively in (a) to (e). Figure 6 is sorted in the same way by Joss as Figure 3 to Figure 5. Where these parameters are indicated again by the color.

https://doi.org/10.5194/egusphere-2024-3840
Preprint. Discussion started: 14 January 2025

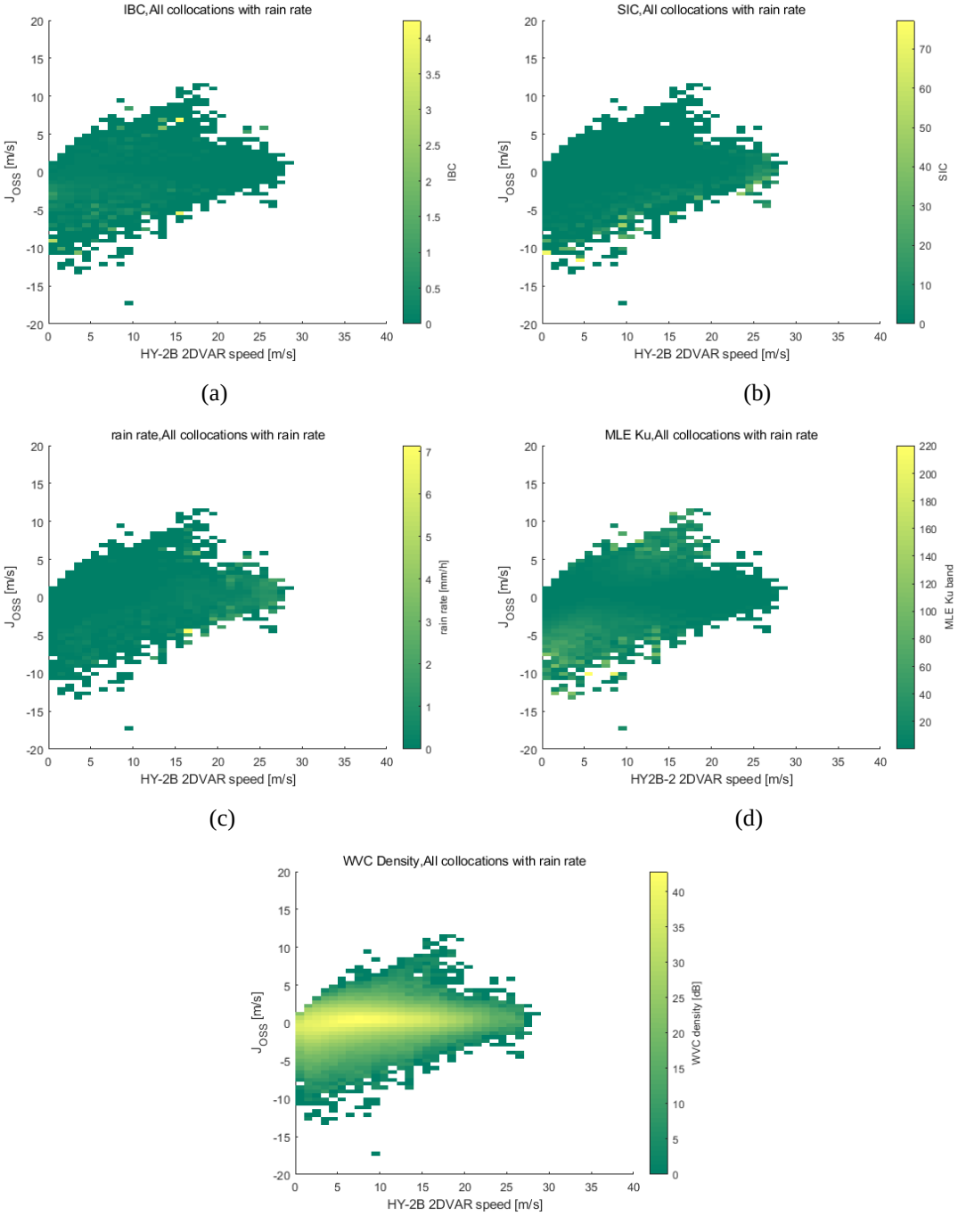

(a) (b) (c) (d) (e)

Figure 6 The distributions of IBC, SIC, rain rate, MLE value and WVC density in (a) – (e) respectively represented by color, the horizontal and vertical axis setting is the same as in Figure 3- Figure 5, where the data is sorted by J_{oss}.

https://doi.org/10.5194/egusphere-2024-3840
Preprint. Discussion started: 14 January 2025

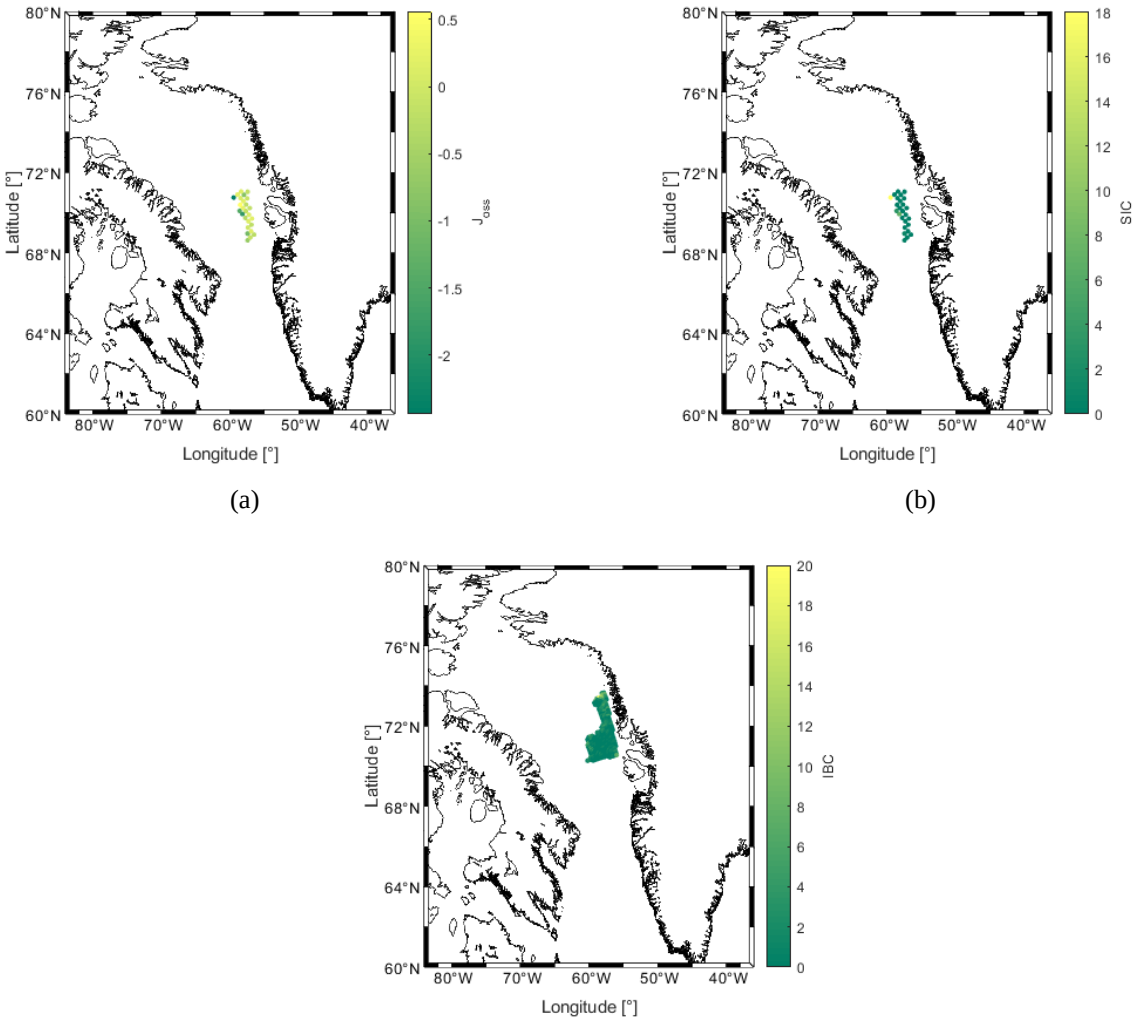

(a) (b)

(c)

Figure 7 A region (M_Map, 2003) selected according to (3), where J_{oss}, SIC and IBC in the color of (a), (b) and (c)

From (d) in Figure 6, the independency to sample numbers is also illustrated. From IBC in (a) and SIC in (b), IBC scatters along different J_{oss} values both below and above 0, with different features from SIC or with rains. When the negative features of IBC overlap slightly with the SIC in (a). While for rains, the consistency to Figure 3-Figure 6 are not broken taken into account the highest rain rate bin obtained in this data set is as low as 7 mm/h, and without general statics compared to the previous figures. Moreover, when comparing (a) and (c), IBC is better resolved by MLE than Joss. This may be induced by that iceberg is allocated in smaller scales than SIC in a WVC. Thus, though iceberg induce larger signal return, they require

https://doi.org/10.5194/egusphere-2024-3840
Preprint. Discussion started: 14 January 2025

better spatial resolution in measurements. This may also be the reason for the positive Joss in a way that a strong NRCS elevates the wind speed than the low-pass filtered 2DVAR speed.

4.3 A case example for further discussion on J_{oss}

From the above, the sea ice screening ability in terms of general SIC of the indicator J_{oss} ensembles that of the rain conditions, discriminates in distribution with speed, while for the iceberg expressed in IBC, the information require finer spatial representation. Meanwhile, from Figure 6, IBC values also demonstrate clustering features along lower J_{oss} values. In this section a case is selected randomly from the criteria applied for rain in (Xu X. and Stoffelen A., 2020), as (3) below, then with the corresponding SIC and IBC values plot for the same region before collocating, and illustrate in Figure 7.

$$J_{oss} \leqslant 0.33\, f - 5 \tag{3}$$

Figure 7 demonstrates a case from the C-and Ku-band collocations chosen randomly and is from the date as the 18th, June, 2018 around 21:55. The J_{oss}, SIC and IBC and values are illustrated with the location with values indicated in colors. The specific location is between Greenland and Canada. The selected WVC can be identified by the grid and red cycle, with locations slightly under the blue line in (a) and (c). According to the color-bar, where the brighter regions in (b) and (c), indicate higher SIC and IBC values. The corresponding J_{oss} in (a) are with a contrasting dark color of low values compared to the surrounding regions and to (b) and (c). The case from Figure 7 confirms the ice screening ability in J_{oss} as well as the potential of iceberg indicating.

5 Conclusion and Discussion

In this research, the sea ice information from scatterometers in spatial distribution and model differences other than direct link from NRCS values to ice properties are investigated in the collocations of C- and Ku-band scatterometers. Reference ice information are SIC from multi-frequency radiometers and IBC from SAR. Rain rates from GPM products are also obtained for the ice screening with discrimination from rains. Analysis of this data set verifies the ice screening ability of J_{oss} and confirms that from MLE with references from wind GMFs for high latitude regions. While Ku band observations are more sensitive to sea ice, concerning not fully ice coverage but SIC values, as well as rain compared to C band, due to their shorter wavelength. When notably, in terms of ice GMF and the relation between C band observations and ice parameters are still valuable among varied remote sensing methods (Belmonte, R. M, et al., 2018).

Specifically, for MLE, it has less screening ability than J_{oss}, but with better consistency to IBC values. values due to their longer wavelength is also concluded. Moreover, for IBC values, MLE values are with better relations than with J_{oss}. This may due to the different features of SIC and IBC when the latter indicate the density of iceberg than the floating ice pieces included in SIC. Icebergs consist a part of sea ice, when IBC is high, the averaged SIC may also not high, vice versa. Moreover, the iceberg alters the return signals in a different way than sea ice distributed over the ocean surface. When the geometry in the elevation may form corner reflectors. And the finer resolution may help getting more information about

https://doi.org/10.5194/egusphere-2024-3840
Preprint. Discussion started: 14 January 2025

them. This can explain that the low-pass filtered J_{oss} illustrate less sensitivity with IBC than MLE. Then the joint application of J_{oss} and MLE is also required considering this.

Specifically, in low to medium wind speed, effects of SIC similar with rains, in higher wind speeds SIC affect more often for high latitude, meanwhile MLE functions well in identifying rains and SIC, both C band and Ku band MLE more sensitive to SIC, IBC than rains. The indicator J_{oss} provides good complementary to MLE metrics. When iceberg is better resolved by MLE, low J_{oss} values are in good consistency in SIC and IBC, a showcase in Figure 7 proves also this. Bayesian scatterometer sea ice screening is operational in MLE in scatterometer wind retrieval, further research of combined applications of the information other than NRCS, as well as their combined application to improve better resolution of ice quantifications. Besides, as the ensembles of rain to SIC, inclusion of precipitation probability could improve ice Bayesian for Ku band. Results can help applications for scatterometers acquiring Ku- and C-band observations at the same time, for example the WindRad onboard FY-3E (Zhang, P. et al., 2024).

Competing interests

The authors declare that they have no conflict of interest.

References

AMSR2: Advanced Microwave Scanning Radiometer 2, instrument details, available online: [https://space.oscar.wmo.int/instruments/view/amsr2]

Belmonte R. M., Otosaka, I., Stoffelen, A., and Verhoef, A.: A scatterometer record of sea ice extents and backscatter: 1992–2016, The Cryosphere, 12, 2941–2953, https://doi.org/10.5194/tc-12-2941-2018, 2018.

Belmonte R. M., Verspeek, J., Verhoef, A., and Stoffelen, A.: Bayesian Sea Ice Detection With the Advanced Scatterometer ASCAT, IEEE Trans. Geosci. Remote Sens., 50(7), 2649–2657, 2012.

Buus-Hinkler, J., Wettre, C., and Hacket, B.: PRODUCT USER MANUAL Icebergs Observed with Sentinel-1 Number Density and Individual Icebergs, document number: SEAICE_ARC_SEAICE_L4_NRT_OBSERVATIONS_011_007, [online accessed] May 2023, https://catalogue.marine.copernicus.eu/documents/PUM/CMEMS-SI-PUM-011-007.pdf.

Drinkwater, M. R., Hosseinmostafa, R., and Gogineni, P.: C-band backscatter measurements of winter sea-ice in the Weddell Sea, Antarctica, Int. J. Remote Sens., 16(17), 3365–3389, 1995.

Frisch, U.: Turbulence: The Legacy of A. N. Kolmogorov, Cambridge University Press, 1995, pp. 72–119.

Haarpaintner, J., Tonboe, R. T., Long, D. G., and Van Woert, M. L.: Automatic Detection and Validity of the Sea-Ice Edge: An Application of Enhanced-Resolution QuikScat/SeaWinds Data, IEEE Trans. Geosci. Remote Sens., 42(7), 1433–1441, July 2004.

https://doi.org/10.5194/egusphere-2024-3840
Preprint. Discussion started: 14 January 2025

Haumann, A: Dynamical Interaction between Atmosphere and Sea Ice in Antarctica, Master's thesis, Utrecht University, Oct. 2011. pp16-21, https://studenttheses.uu.nl/handle/20.500.12932/15257

Huffman, G. J., Bolvin, D. T., and Nelkin, E. J.: "Integrated Multi-satellite Retrievals for GPM (IMERG) technical documentation," NASA/GSFC Code, vol. 612, p. 47, Jun. 2015.

HY-2B: Satellite details, available online: https://space.oscar.wmo.int/satellites/view/hy_2b.

Lindell, D. B., and Long, D. G.: Multiyear Arctic Sea Ice Classification Using OSCAT and QuikSCAT, IEEE Trans. Geosci. Remote Sens., 54(1), 167–175, https://doi.org/10.1109/TGRS.2015.2452215, Jan. 2016 a.

Lindell, D.B. and Long, D.G. Multiyear Arctic Ice Classification Using ASCAT and SSMIS. Remote Sens. 2016 b, 8, 294. https://doi.org/10.3390/rs8040294

M_Map: A mapping package for MATLAB," 2023. [Online]. Available: http:// www.eoas.ubc.ca/ ~rich/map.html. [Accessed: Nov. 26, 2024].

Melsheimer, C.: ASI Version 5 Sea Ice Concentration User Guide, Technical Report, V0.8.0, October 30, 2018, https://seaice.uni-bremen.de/data/Documents/ASIuserguide.pdf.

Otosaka, I., Belmonte Rivas, M., and Stoffelen, A.: Bayesian Sea Ice Detection With the ERS Scatterometer and Sea Ice Backscatter Model at C-Band, IEEE Trans. Geosci. Remote Sens., 56(4), 2248–2254, 2018.

Pistone, K., Eisenman, I., and Ramanathan, V.: Observational determination of albedo decrease caused by vanishing Arctic sea ice, Proc. Natl. Acad. Sci. U.S.A., 111(9), 3322–3326, https://doi.org/10.1073/pnas.1318201111, 2014.

Portabella, M., and Stoffelen, A.: Characterization of residual information for SeaWinds quality control, IEEE Trans. Geosci. Remote Sens., 40(12), 2747–2759, 2002.

Portabella, M., Stoffelen, A., Verhoef, A., and Verspeek, J.: ASCAT Scatterometer Wind Quality Control, presented at EUMETSAT Satellite Conference, EUMETSAT, Córdoba, Spain, 2010. https://cdn.knmi.nl/system/data_center_publications/files/000/068/708/original/paper_ascat_qc_eumetsat2010.pdf?1495621340

Portabella, M.: Wind Field Retrieval from Satellite Radar Systems, Ph.D. thesis, Ph.D. program in Astronomy and Meteorology, University of Barcelona, 2002. Available online: https://digital.csic.es/bitstream/10261/154354/1/Portabella_thesis_2002.PDF.

Ricciardulli, L., and Wentz, F. J.: A Scatterometer Geophysical Model Function for Climate-Quality Winds: QuikSCAT Ku-2011, J. Atmos. Oceanic Technol., 32(10), 1829–1846, https://doi.org/10.1175/jtech-d-15-0008.1, 2015.

Sandven, S., Johannessen, O. M., and Kloster, K.: Sea Ice Monitoring by Remote Sensing, Encyclopedia of Analytical Chemistry, Vol. 6, Chapter 8, John Wiley & Sons, September 2006, https://doi.org/10.1002/9780470027318.a2320.

Sandven, S., Spreen, G., Heygster, G. et al. Sea Ice Remote Sensing—Recent Developments in Methods and Climate Data Sets. Surv Geophys 44, 1653–1689 (2023). https://doi.org/10.1007/s10712-023-09781-0

Sentinel-1: Satellite Programme details, available online: [https://space.oscar.wmo.int/satelliteprogrammes/view/sentinel_1]

https://doi.org/10.5194/egusphere-2024-3840
Preprint. Discussion started: 14 January 2025

Siedler, G., Church, J., and Gould, J. (Eds.): Ocean Circulation and Climate: Observing and Modeling the Global Ocean, International Geophysics Series, Vol. 77, Academic Press, 2001, pp. 200-400, ISBN 9780126413519.

Stoffelen, A. and Verhoef A.: Advances in Ku-band Scatterometer Quality Control, Version 1.1, OSI SAF Technical Note, OSISAF_CDOP3_SS3_TN, 15 Sept. 2021. Available online: https://cdn.knmi.nl/system/data_center_publications/files/000/072/067/original/osisaf_cdop3_ss3_tn_advances_in_ku-band_qc_1.1.pdf?1704987969.

Stoffelen, A., Verspeek, J. A., Vogelzang, J., and Verhoef, A.: The CMOD7 Geophysical Model Function for ASCAT and ERS Wind Retrievals, IEEE J. Sel. Top. Appl. Earth Obs. Remote Sens., 10(5), 2123–2134, https://doi.org/10.1109/jstars.2017.2681806, 2017

Stoffelen, A.: Scatterometry, Ph.D. thesis, University of Utrecht, ISBN 90-393-1708-9, October 1998. Available online: https://dspace.library.uu.nl/bitstream/handle/1874/636/full.pdf.

Timmermans, M.-L., and Marshall, J.: Understanding Arctic Ocean Circulation: A Review of Ocean Dynamics in a Changing Climate, J. Geophys. Res. Oceans, 125, https://doi.org/10.1029/2018JC014378, 2020.

Verhoef, A., and Stoffelen, A.: Quality Control of Ku-band Scatterometer Winds, Ocean and Sea Ice SAF Technical Note, SAF/OSI/CDOP2/KNMI/TEC/RP/194, Version 1.0, KNMI, March 2012. Available online: http://knmi-scatterometer-website-prd.s3.amazonaws.com/publications/ku_band_qc_1.0.pdf.

Verhoef, A., Vogelzang, J., Verspeek, J., and Stoffelen, A.: "PenWP Top Level Design," KNMI, De Bilt, the Netherlands, Tech. Rep. NWPSAF-KN-DS-001, Version 2.1, Feb. 2017. [Online]. Available: [https://cdn.knmi.nl/system/data_center_publications/files/000/070/108/original/nwpsafknds001_penwp_topleveldesign_v2.1.pdf?1495622157].

Vogelzang, J., and Stoffelen, A.: Scatterometer wind vector products for application in meteorology and oceanography, J. Sea Res., 74, 16–25, https://doi.org/10.1016/j.seares.2012.05.002, 2012.

Vogelzang, J., Stoffelen, A., Verhoef, A., and Figa-Saldaña, J.: On the quality of high-resolution scatterometer winds, HJ. Geophys. Res., 116, C10033, doi:10.1029/2010JC006640, 2011.

Vogelzang, J.: Two dimensional variational ambiguity removal (2DVAR), KNMI Tech. Note NWP SAF NWPSAF-KN-TR-004, 2017. Accessed: May 3, 2019. [Online]. Available: http://citeseerx.ist.psu.edu/viewdoc/download;jsessionid=88BBD01BAD28915EE1C4869F66E91F73?doi=10.1.1.627.1963&rep=rep1&type=pdf.

Wang, Z., Stoffelen, A., Zhao, C., et al.:"An SST-dependent Ku-band geophysical model function for RapidScat," Journal of Geophysical Research: Oceans, 122(4), p. 3461-3480, 2017.

https://doi.org/10.5194/egusphere-2024-3840
Preprint. Discussion started: 14 January 2025

Wentz, F. J., Mattox, L. A., and Peteherych, S.: A Model Function for Ocean Radar Cross-sections at 14.6 GHz, J. Geophys. Res., 89, 3689–3704, May 20, 1984.

Wernecke, A., Notz, D., Kern, S., and Lavergne, T.: Estimating the uncertainty of sea-ice area and sea-ice extent from satellite retrievals, The Cryosphere, 18, 2473–2486, https://doi.org/10.5194/tc-18-2473-2024, 2024.

Woodhouse, I. H.: Introduction to Microwave Remote Sensing, 1st Ed., CRC Press, 2006, pp. 133–138. ISBN 9780367225148.

Xu, X., and Stoffelen, A.: Improved Rain Screening for Ku-Band Wind Scatterometry, IEEE Trans. Geosci. Remote Sens., 58(4), 2494–2503, https://doi.org/10.1109/tgrs.2019.2951726, 2020.

Xu, X., Stoffelen, A., and Meirink, J. F.: "Comparison of Ocean Surface Rain Rates From the Global Precipitation Mission and the Meteosat Second-Generation Satellite for Wind Scatterometer Quality Control," IEEE Journal of Selected Topics in Applied Earth Observations and Remote Sensing, vol. 13, pp. 2173-2182, 2020. doi: 10.1109/igarss47720.2021.9553678.

Xu, X., Stoffelen, A., Portabella, M., Lin, W., and Dong, X.: A Comparison of Quality Indicators for Ku-Band Wind Scatterometry & for Typhoons Lekima and Krosa, IEEE International Geoscience and Remote Sensing Symposium, 2021, https://doi.org/10.1109/igarss47720.2021.9553678.

Zhang, P., Hu, X., Sun, L., Xu, N., Chen, L., Zhu, A., Lin, M., Lu, Q., Yang, Z., Yang, J., and Wang, J.: "The On-Orbit Performance of FY-3E in an Early Morning Orbit," Bulletin of the American Meteorological Society, vol. 105, no. 1, pp. E144–E175, 2024. doi: [10.1175/bams-d-22-0045.1](https://doi.org/10.1175/bams-d-22-0045.1).